PNAS RESEARCH ARTICLE | PHYSICS

Non-Fermi liquid phase and linear-in-temperature scattering rate in overdoped two-dimensional Hubbard model

Wéi Wú[a,1], Xiang Wang[a], and André-Marie Tremblay[b]

Edited by J. C. Davis, University of Oxford, Oxford, United Kingdom; received August 27, 2021; accepted February 18, 2022

Understanding electronic properties that violate the Landau Fermi liquid paradigm in cuprate superconductors remains a major challenge in condensed-matter physics. The strange metal state in overdoped cuprates that exhibits linear-in-temperature scattering rate and direct current (dc) resistivity is a particularly puzzling example. Here, we compute the electronic scattering rate in the two-dimensional Hubbard model using cluster generalization of dynamical mean-field theory. We present a global phase diagram documenting an apparent non-Fermi liquid phase, in between the pseudogap and Fermi liquid phase in the doped Mott insulator regime. We discover that in this non-Fermi liquid phase, the electronic scattering rate $\gamma_k(T)$ can display linear temperature dependence as temperature T goes to zero. In the temperature range that we can access, the T-dependent scattering rate is isotropic on the Fermi surface, in agreement with recent experiments. Using fluctuation diagnostic techniques, we identify antiferromagnetic fluctuations as the physical origin of the T-linear electronic scattering rate.

strange metal | Hubbard model | cuprate | dynamical mean-field theory | superconductivity

Significance

Most metals display an electron-scattering rate $1/\tau$ that follows $1/\tau \sim T^2$ at low temperatures, as prescribed by Fermi liquid theory. But there are important exceptions. One of the most prominent examples is the "strange" metal regime in overdoped cuprate supercondcutors, which exhibits a linear T dependence of the scattering rate $1/\tau \sim T$ that reaches a putative Planckian limit. Here, using cutting-edge computational approaches, we show that T-linear scattering rate can emerge from the overdoped Hubbard model at low temperatures. Our results agree with cuprate experiments in various aspects but challenge the Planckian limit. Finally, by identifying antiferromagnetic fluctuations as the physical origin of the T-linear scattering rate, we discover the microscopic mechanism of strange metallicity in cuprates.

The non-Fermi liquid states emerging from strongly correlated electron systems have been one of the central research topics in condensed-matter physics (1). One of the most profound problems in this field is the strange metal state in cuprates, characterized by a linear temperature dependence of direct current (dc) resistivity, and a scattering rate $1/\tau$ reaching a putative universal "Planckian limit," $\hbar/\tau = k_B T$ (2–7). Since the discovery of strange metallicity in cuprates (8–10) and other materials (4, 11–13), enormous effort has been aimed at tracing its physical origin, including phenomenological theories (14, 15); considerations on quantum critical fluctuations in the vicinity of a quantum critical point (QCP) (16–22); and also studies of microscopic models (23, 24) in the absence of a nearby QCP, such as the Sachdev–Ye–Kitaev (SYK)-type models with random interactions (23–25). To date, however, the rigorous relevance of these models to overdoped cuprates is still far from clear, since little is known about the underlying mechanism of the strange metal state.

The two-dimensional Hubbard model, which is prevalent in modeling correlated materials, can capture various signature features of hole-doped cuprates, such as d-wave superconductivity (26–29), pseudogap (30–35), and stripe order (36, 37). Recently, in studies at very high temperatures ($T \sim$ bandwidth W), the so-called "bad metal" regime of the Hubbard model has been reported (38–41). In those studies, the high-temperature T-linear resistivity stems largely from a change in effective carrier number with temperature (40, 42). This is in stark contrast to cuprate materials, where the T-linear dc resistivity occurs at low temperature, the so-called "strange metal" regime. In this regime, it is argued that linear-in-temperature resistivity originates from a scattering rate $1/\tau$ that scales linearly with temperature (43) and reaches a putative fundamental limit set by "Planckian dissipation" (3). Whether the Hubbard model can provide a proper description of the cuprate strange metal at low temperatures is therefore still a crucial open question.

To address these problems, in this work we solve the two-dimensional Hubbard at low temperatures on a square lattice, in the doped Mott-insulator regime using the dynamical cluster approximation (DCA) (44). We demonstrate that the T-linear electronic scattering rate at low temperatures, found in the strange metal state of hole-doped cuprates (2, 45), can emerge from the overdoped Hubbard model. The inelastic part of the T-linear electronic scattering rate is the same at the node and at the antinode. Our results suggests that although the scattering rate is close to the Planckian one, that rate does not seem to be a limit for reasons that we explain. More importantly, we explicitly identify that short-ranged antiferromagnetic correlations, despite being greatly suppressed in the overdoped regime, are at the origin of the T-linear scattering rate characterizing strange metallicity.

We consider the Hubbard model Hamiltonian,

$$\mathcal{H} = \sum_{ij,\sigma} -t_{ij}\, c^{\dagger}_{i,\sigma} c_{j,\sigma} + U \sum_{i} n_{i\uparrow} n_{i\downarrow} - \mu \sum_{i,\sigma} n_{i\sigma}, \qquad [1]$$

Author contributions: W.W. designed research; W.W. performed research; X.W. contributed new reagents/analytic tools; W.W. and A.-M.T. analyzed data; and W.W. and A.-M.T. wrote the paper.

The authors declare no competing interest.

This article is a PNAS Direct Submission.

[1]To whom correspondence may be addressed. Email: wuwei69@mail.sysu.edu.cn.

This article contains supporting information online at https://www.pnas.org/lookup/suppl/doi:10.1073/pnas.2115819119/-/DCSupplemental.

Published March 23, 2022.

where μ is the chemical potential, and the t_{ij} s are nonzero for nearest-neighbor hoppings t and next–nearest-neighbor hoppings t', which vary in different cuprate compounds (46). U is the onsite Coulomb repulsion, which is taken as $U/t = 7$ throughout this work. We work in units where $t = 1$, the lattice spacing, Boltzmann's constant k_B, and Planck's constant $\hbar$ are also set equal to unity. The DCA method is a cluster extension of the dynamical mean-field theory (DMFT) (47) that treats quantum and short-ranged spatial correlations exactly, while longer-range correlations beyond the cluster are incorporated in a dynamical mean-field way (*Materials and Methods*).

Results

Phase Diagram. We first display two characteristic energy scales of the doped normal-state Hubbard model, the pseudogap temperature T^* and the Fermi liquid temperature T_{FL}, as a function of doping levels p in Fig. 1*A*. Here T^* is defined as the temperature T where the antinodal zero-frequency spectral function starts to decrease with T, and T_{FL} is identified as the temperature where the paramagnetic susceptibility (Knight shift) becomes T independent (*SI Appendix*, Fig. S4). Extrapolating T^* and T_{FL} to zero, one finds two critical dopings: p^*, where the pseudogap disappears for $p > p^*$, and p_{FL} where Fermi liquid emerges for $p > p_{FL}$. Repeating this calculation for several t' values, we obtained a zero-temperature phase diagram in the $p - t'$ plane, as shown in Fig. 1*B*, which consists of three different phases: 1) the pseudogap (PG) phase in the underdoped regime where $p < p^*$ (and $T^* > 0$); 2) the canonical Fermi liquid (FL) phase on the heavily overdoped side for $p > p_{FL}$ (where $T_{FL} > 0$); and finally 3) in between the PG and FL phases, there exists a non-Fermi liquid (NFL) phase where the extrapolated T^* and T_{FL} both vanish in the $p^* < p < p_{FL}$ interval. Namely in the NFL phase, there is no pseudogap at the Fermi level but the physical properties disagree with expectations for a Fermi liquid. It is remarkable that for all the t' values we have studied, the NFL resides in a finite range of dopings. In fact, as the value of $|t'/t|$ increases, the NFL regime becomes broader in doping, as one can see from Fig. 1*A*. This result suggests that upon hole doping, the pseudogap state does not directly transit to the Fermi liquid phase via a single quantum critical point at zero temperature.*

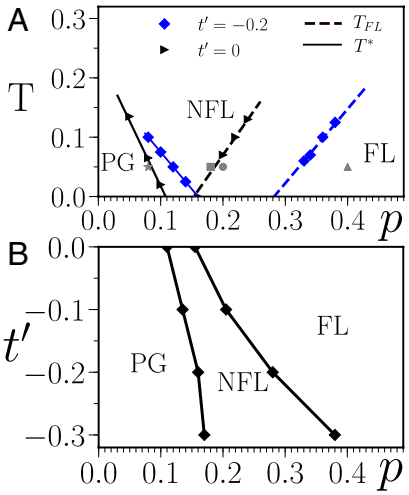

Fig. 1. PG, NFL, and FL phases of the doped Hubbard model in normal state. (*A*) Pseudogap temperature T^* and Fermi liquid temperature T_{FL} as a function of hole-doping value p for two typical t' values, $t' = 0$ (triangles) and $t' = -0.2$ (diamonds). The finite-temperature data points are extrapolated to zero temperature (lines), yielding two critical dopings p^* and p_{FL}. For example, for $t' = -0.2$, $p^* \simeq 0.16$ and $p_{FL} \simeq 0.28$. For the definition of T^* and T_{FL} please refer to main text and *SI Appendix*, section C. The gray symbols mark the data points that are further analyzed in Fig. 4 at $t' = -0.2t$. (*B*) Zero-temperature phase diagram in the $p - t'$ plane. The above extrapolated p^* and p_{FL} define the PG/NFL and NFL/FL phase boundaries, respectively.

Comparing with experiments, we note that in the $La_{2-x}Sr_xCuO_4$ (LSCO) compound ($t'/t \sim -0.2$), it is found that the PG ends at $p^* \simeq 0.18$, and Fermi liquid shows up at $p_{FL} \simeq 0.3$ [where p_{FL} is defined as where the temperature-dependent resistivity becomes $\rho(T) \propto T^2$ (8, 48)]. This is in good agreement with our result that the NFL exists in the doping range $p \in (p^* = 0.16, p_{FL} = 0.28)$ at $t'/t = -0.2$. Recall that here the spontaneous symmetry-breaking phases, such as the d-wave superconductivity (SC), are suppressed to simulate transport experiments in a high magnetic field.

***T*-Linear Scattering Rate.** The electronic scattering rate $\gamma_k \equiv -\mathrm{Im}\Sigma(k, \omega = 0)$ in the NFL phase is the primary focus of this work. We find that in the NFL, the Matsubara data for the self-energy $\Sigma(\mathbf{k}, i\omega_n)$ are consistent with the hypothesis that the imaginary part of the self-energy in real frequency space $\Sigma''(k, \omega) \equiv \mathrm{Im}\Sigma(k, \omega)$ follows an ω/T scaling (14, 25, 49–51) at low energies (*SI Appendix*, Figs. S5 and S6). Hence, we assume that $\Sigma''(k, \omega)$ can be written as $\Sigma''(k, \omega) = -T^\alpha \phi(\omega/T) - b$ (45, 50) at low energies, where $\phi(\omega/T)$ is an analytic function of ω/T, while α and b are constants. With this assumption, the imaginary part of the self-energy at zero frequency that follows from a second-order polynomial extrapolation in Matsubara frequencies $\gamma'_k \equiv -\mathrm{Im}\Sigma^{(2)}(k, \omega = 0) = -\mathrm{Im}[1.875\Sigma(k, i\omega_0) - 1.25\Sigma(k, i\omega_1) + 0.375\Sigma(k, i\omega_2)] = aT^\alpha + b$ will have exactly the same T dependence of the true scattering rate γ_k, since the scaling hypothesis implies that $\gamma_k = \phi(0)T^\alpha + b$. Therefore, one can find the exact exponent α describing the T dependence of γ_k from analyzing the γ'_k data, despite the fact that the fit leaves the constant coefficient $\phi(0)$ unknown [if $\Sigma''(k, \omega)$ is $\omega-$independent over the frequency range $|\omega| \lesssim 4T$, $\phi(0) \approx a$; see *SI Appendix*, section D for details].

Throughout the following, we use the typical value $t' = -0.2$ as an example to study the T-linear scattering rate. Fig. 2 displays γ'_k as a function of temperature T for different p values, where one can see that at high temperatures, the scattering rate γ'_k is linear in temperature in a remarkably large doping range, from an underdoped ($p = 0.12$, Fig. 2*A*) to a heavily overdoped side ($p = 0.34$, Fig. 2*G*) (48).

When T is decreased, focusing on the antinodal γ'_k at $\mathbf{k} = (0, \pi)$ as shown in Fig. 2 *A* and *B*, at small dopings ($p = 0.12, 0.14$, in the PG), γ'_k deviates from its high-temperature T linearity, developing a prominent upturn when the pseudogap temperature T^* is reached. This resembles the upturn seen in the dc resistivity curves in transport experiments (52) and in other calculations (53, 54), which characterizes the opening of the pseudogap. As the doping level p increases, the upturn of γ'_k at the antinode shifts to lower temperatures in the PG phase, reflecting the decreasing T^*. Finally, when the NFL phase is reached, a possible upturn of γ'_k moves outside of the accessible temperature range. The linear T dependence of γ'_k at the antinode extends to $T \to 0$, as shown in Fig. 2*D*. For the node, γ'_k preserves the linear-in-T behavior, crossing the PG–NFL transition. Thus, for a typical doping close to p^* in the NFL, $p = 0.18$ (Fig. 2*D*) for example, both the node and the antinode display a T-linear

*The first-order transition found in Sordi et al. (32) is related to the end of the pseudogap regime. At larger doping, a correlated metal phase is found in that work, but how the crossover to the Fermi liquid occurs was not investigated.

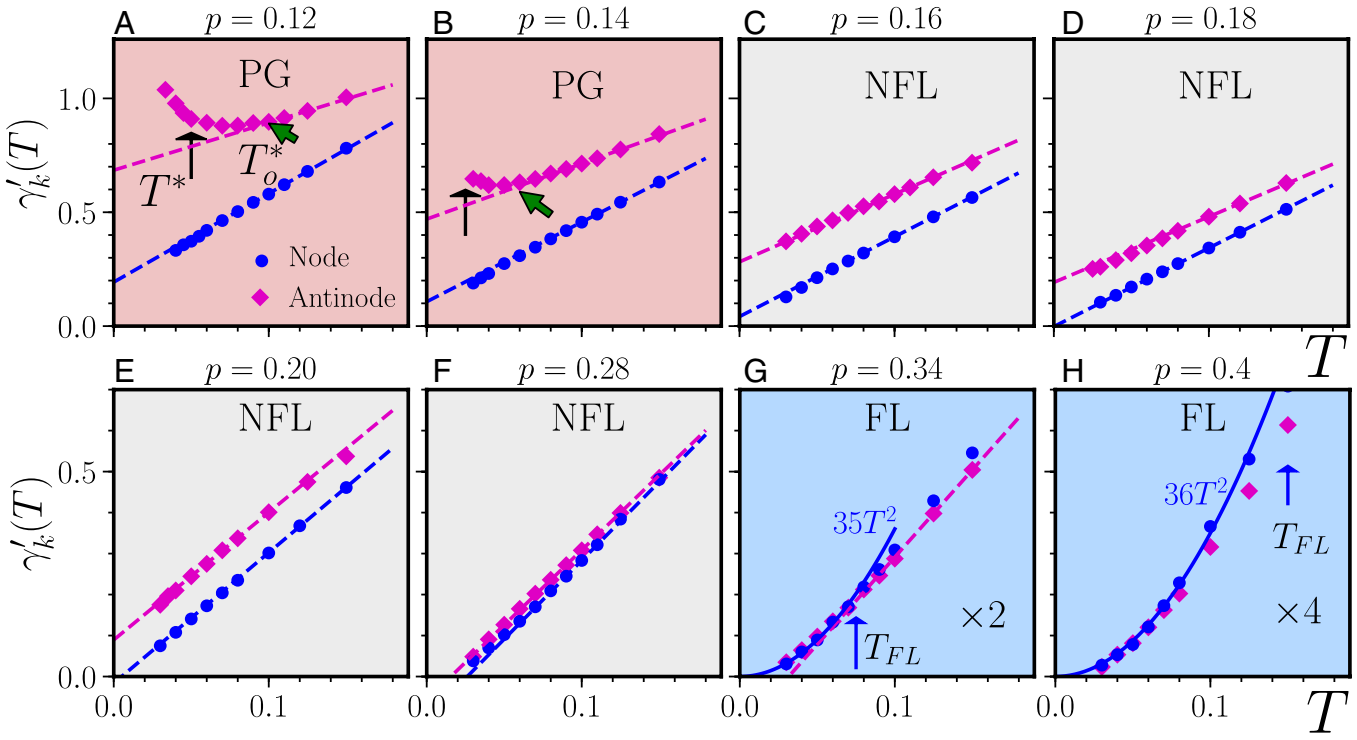

Fig. 2. (*A–H*) Temperature dependence of the electron-scattering rate. Here $\gamma_k' \equiv -\mathrm{Im}\Sigma^{(2)}(k, \omega = 0)$ is shown as a function of temperature T for different dopings. Dashed lines show linear fittings $\gamma_k' = aT + b$, while solid lines show quadratic fittings $\gamma_k' = aT^2$. For example, at $p = 0.18$, for antinode $\gamma_k' \approx 3.13T + 0.17$ and for node $\gamma_k' \approx 3.45T$, while $\gamma_k' \approx 9T^2$ for nodal γ_k' at $p = 0.4$. Note that in *G* and *H*, γ_k' data are enlarged for clarity. The pseudogap temperature T^* and the temperature T_o^* where γ_k' starts to deviate from linearity are marked by arrows in *A* and *B*. In *G* and *H* the Fermi liquid temperature (T_{FL}) is also indicated by arrows. For the definition of T^* and T_{FL}, please refer to main text and *SI Appendix*, section C.

scattering rate in the full temperature regime. On the heavily overdoped side, the Landau Fermi liquid paradigm is restored at small T when $p > p_{FL}$. As shown in Fig. 2 *G* and *H*, the scattering rates cross over from high T linearity to a clear T-square behavior (55) as $T < T_{FL}$.

In essence, at low dopings γ_k' has upturns that characterize the PG, while at large dopings it follows the T^2 law that characterizes the FL. In the NFL, where T^* and T_{FL} are both vanishingly small, $\gamma_k'(T)$ obeys $\gamma_k'(T) = aT + b$ in a broad T range. Nevertheless, we point out that in the NFL, when doping p is close to p^* or p_{FL}, the precursor effects of pseudogap or Fermi liquid at small T can also break the T linearity of $\gamma_k'(T)$, even if T^* or T_{FL} appears to vanish (*SI Appendix*, Fig. S7). As a result, in the $T \to 0$ limit, $\gamma_k'(T) = aT + b$ is obeyed only in a part of the NFL regime. For example, at $t'/t = -0.2$, while our definition suggests that the NFL exists in $0.16 \lesssim p \lesssim 0.28$ at vanishing T (see discussions in *SI Appendix*, section E), the perfect linear-in-T behavior of $\gamma_k'(T)$ [or equivalently the linear-in-T behavior of $\gamma_k(T)$] occurs in the doping range of $0.17 \lesssim p \lesssim 0.20$ as $T \to 0$.

Up to now, we have investigated the electron-scattering rate $\gamma_k = -\mathrm{Im}\Sigma(k, \omega = 0)$. In the FL regime, this differs from the quasiparticle scattering rate by a temperature-independent quasiparticle weight z_k. In the NFL regime, it is worthwhile to investigate the phenomenological marginal Fermi liquid (MFL) interpretation of the scattering rate $1/\tau_k = z_k\gamma_k$ with $\gamma_k = -\mathrm{Im}\Sigma(\mathbf{k}, \omega) = \alpha \max(|\omega|, \pi T) + b$ (5, 14). The procedure for finding τ_k from fitting the Matsubara Green's function is explained in *SI Appendix*, section F. We find $1/\tau_k \sim CT$, with $C \in (1 \sim 2)$ (*SI Appendix*, Figs. S8–S10) for two doping levels, $p = 0.18$ and $p = 0.2$, in the T-linear regime. We stress that here C is found dependent on doping p and momentum $\mathbf{k}$. It decreases as p increases, contrary to what we found for the electron-scattering rate, which is nearly independent of doping in the NFL regime.

Origin of the NFL and *T* Linearity. To reveal the physical origin of the T-linear scattering rate in the overdoped Hubbard model, we turn to the fluctuation diagnostic technique (56), which uses the Dyson–Schwinger equation of motion (DSEOM) to decompose the self-energy at the two-particle level (56–59). Simply explained, the essential idea of this approach is to find how collective modes in different channels [spin (sp), charge (ch), or particle–particle (pp)] contribute to the self-energy. As depicted by the Feynman diagram for the spin channel in Fig. 3 *B*, *Inset*, the self-energy (with Hartree term $Un/2$ subtracted) can be written as (56)

$$\Sigma(k) - \frac{Un}{2} = -\frac{U}{g(k)\beta^2 N}\sum_{k',Q} F_{sp}(k, k', Q)g(k')g(k)g(k'+Q)g(k+Q), \quad [2]$$

where wavevectors k stand for $k = (\mathbf{k}, i\omega_n)$ and $g(k)$ is the full single-particle Green's function. Here F_{sp} is the full two-particle scattering amplitude in the transverse spin channel. Hence the right-hand side of Eq. **2** can be rewritten in terms of the spin operators $S_k^+(-Q) = C_{k\uparrow}^\dagger C_{k+Q,\downarrow}$ and $S_{k'}^-(Q) = C_{k'+Q\downarrow}^\dagger C_{k',\uparrow}$,

$$\Sigma(k) - \frac{Un}{2} = \frac{-U}{g(k)\beta^2 N}\sum_{k',Q}\langle S_k^+(-Q)S_{k'}^-(Q)\rangle \quad [3]$$

and we can introduce a new quantity $\Sigma_{sp}^Q(k) = [-U/g(k)]\sum_{k'}\langle S_k^+(-Q)S_{k'}^-(Q)\rangle$ such that $\Sigma(k) - Un/2 = \sum_Q \Sigma_{sp}^Q(k)$, which has a clear physical meaning: The ratio $|\mathrm{Im}\Sigma_{sp}^Q(k)/\mathrm{Im}\Sigma(k)|$

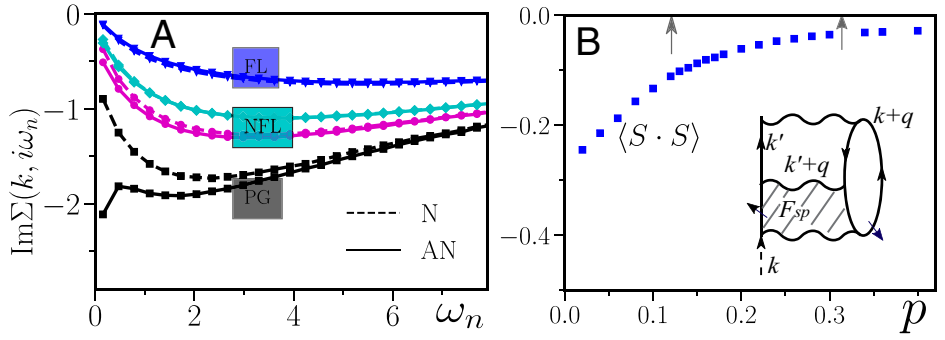

Fig. 3. Imaginary part of the self-energy in PG, NFL, and FL phases and the spin–spin correlator $\langle S_i \cdot S_{i+1} \rangle$ on nearest-neighboring sites $\langle i, i+1 \rangle$ as a function of doping p. (*A*) $\mathrm{Im}\Sigma(k, i\omega_n)$ as a function of ω_n. From bottom to top, $p = 0.08$ (PG); $p = 0.18$, $p = 0.24$ (NFL); and $p = 0.4$ (FL). (*B*) Spin correlator $\langle S_i \cdot S_{i+1} \rangle$ at two neighboring sites $(i, i+1)$ as a function of doping p. Two arrows indicate PG/NFL and NFL/FL phase boundaries, respectively. (*Inset*) Feynman diagram that sketches the DSEOM decomposition of the self-energy in the spin channel. Here $U = 7t$, $t' = -0.2t$, $T = 0.05t$.

tracks the relative importance of the spin excitation with the momentum/frequency transfer Q to the electronic scattering. The above analysis can also be straightforwardly applied to charge and particle–particle representations to estimate the impacts of the corresponding two-particle excitations on the self-energy (*SI Appendix*, section I).

In Fig. 3*A*, $\mathrm{Im}\Sigma(\mathbf{k}, i\omega_n)$ is shown as a function of ω_n in different states. Focusing on the low-energy scattering, we perform the fluctuation diagnostic on the imaginary part of the self-energy at the first fermionic Matsubara frequency $\mathrm{Im}\Sigma(k, i\omega_0)$. The decompositions in the spin channel, $\mathrm{Im}\Sigma^{Q}_{sp}(\mathbf{k}, i\omega_0)$ is displayed in Fig. 4, as a function of $Q = (\mathbf{q}, i\Omega_n)$ for two typical dopings in the T-linear regime in NFL, $p = 0.18, 0.2$. For comparison, the results at $p = 0.08$ (PG) and $p = 0.4$ (FL) are also shown.

We consider first the $p = 0.18$ case. For both antinode [$\mathbf{k} = (0, \pi)$, Fig. 4 *A2*] and node [$\mathbf{k} = (\pi/2, \pi/2)$, Fig. 4 *B2*], $-\mathrm{Im}\Sigma^{\mathbf{q}}_{sp}(\mathbf{k}, i\omega_0)$ at different $\mathbf{q}$ is extremely uneven. The antiferromagnetic (AFM) wavevector $\mathbf{q} = (\pi, \pi)$ component accounts for most of the low-energy scattering $-\mathrm{Im}\Sigma(\mathbf{k}, i\omega_0)$. This means that in the NFL, most of the electronic scatterings are due to AFM fluctuations, since $\Sigma^{\mathbf{q}}_{sp}(k) \propto \sum_{k'} \langle S^{+}_{k}(-\mathbf{q}) S^{-}_{k'}(\mathbf{q}) \rangle$. Moreover, from Fig. 4 *C2*, one learns from the frequency decomposition that the $\Omega = 0$ component dominates, suggesting the long-lived nature of the well-defined AFM fluctuations at this doping.

At a larger doping $p = 0.20$, the weight of the $\mathbf{q} \neq (\pi, \pi)$ components grows, as shown in Fig. 4 *A3* and *B3*. However, the predominant role of the $\mathbf{q} = (\pi, \pi)$ mode is not changed. In fact, we find that the $\mathbf{q} = (\pi, \pi)$ component always has the largest contribution to $-\mathrm{Im}\Sigma^{\mathbf{q}}_{sp}(\mathbf{k}, i\omega_0)$ among different $\mathbf{q}$ in the NFL, even when p is further increased (*SI Appendix*, Fig. S15).[†] This result is somewhat surprising, as one would intuitively expect negligible AFM correlations in the overdoped regime. To clarify this problem, in Fig. 3*B* we plot the spin–spin correlator $\langle S_{i+1} \cdot S_i \rangle$ between a pair of neighboring sites $(i, i+1)$ as a function of doping p. This shows that, although largely reduced by doping, the strength of AFM correlations remains significantly nonzero in the NFL. For example, at $p = 0.2$, $\langle S_{i+1} \cdot S_i \rangle \approx -0.06$, which is about 40% of the value at $p = 0.08$ in the PG. Neutron-scattering studies on LSCO show that at $p = 0.25$ in the NFL, the dynamical magnetic susceptibility still has fairly large intensity at finite energy, whose magnitude is about half of that at $p = 0.125$ in the PG (60). Resonant inelastic scattering studies also reveal the persistence of spin excitations in the overdoped regime (61). This emphasizes again that the short-ranged AFM correlations should not be overlooked in the overdoped regime.

The decompositions for the PG and the FL are shown, respectively, in Fig. 4, *Left* and *Right* columns. In the PG, $-\mathrm{Im}\Sigma^{Q}_{sp}(\mathbf{k}, i\omega_0)$ is similar to the NFL case, revealing again the importance of scattering off AFM fluctuations (52, 56, 57). By contrast, in the FL phase, a clear distinction between the NFL and PG cases is observed: $-\mathrm{Im}\Sigma^{\mathbf{q}/\Omega_n}_{sp}(k)$ with different $\mathbf{q}/\Omega_n$ are more or less comparable. There is no individual mode in $\mathbf{q}/\Omega_n$ space that provides a dominant contribution to scattering. This is expected, since scattering in Fermi liquids should be seen as single-particle collisions rather than scattering off collective modes. Hence the two-particle spin representation becomes inappropriate to identify the source of scattering in the FL.

We also performed DSEOM decompositions in other channels and found no indication of any significant charge or particle–particle collective modes in the NFL (*SI Appendix*, section I and Fig. S13). Therefore, we conclude that in the NFL, most of the T-linear electronic scattering comes from AFM fluctuations.

Discussion

In recent angle-resolved photoemission spectroscopy (ARPES) measurements of Bi2212, it is found that the ARPES spectra near p^* can be well fitted by a marginal Fermi liquid form for the self-energy $-\mathrm{Im}\Sigma(k, \omega) = T\phi(\omega/T) + b$ (45), which supports our assumption of ω/T scaling in the NFL state. Moreover, we note that $\gamma'_k(T)$ has similar slopes in T at the node and at the antinode, which means that the inelastic part (T-dependent part) of the scattering rates, $\gamma^{in}_k(T) \equiv \gamma'_k(T) - \gamma'_k(0)$, is isotropic in our study. For example, at $p = 0.18$, $\gamma^{in}_N(T)/\gamma^{in}_{AN}(T) \approx 1.1$, as shown in Fig. 2. This agrees with early ARPES results (62) and very recent angle-dependent magnetoresistance (ADMR) experiments on LSCO (43). We note that an immediate consequence of $\gamma_k(T)$ being perfectly linear in T in the NFL is that the dc resistivity ρ_T without vertex corrections can also have linear temperature dependence, since the band dispersion is found T independent here (*SI Appendix*, section G).

This is in contrast to the T-linear dc resistivity found in previous studies on the doped Hubbard model at high temperatures (40, 55, 63) or in some studies of SYK models (25, 64), where the effective band dispersion does bring T dependence to the dc resistivity.

Finally, we emphasize that in our study no specific functional form of the self-energy is assumed, except a generic ω/T scaling. It is notable that a previous DCA study (65) assuming the MFL type of self-energy on the doped Hubbard model at smaller U and higher temperatures suggested a finite-temperature MFL regime

[†]We have checked that the spin structure factor $\langle S(-q)S(q) \rangle$ remains short range despite the large peak at $q = (\pi, \pi)$ in $-\mathrm{Im}\Sigma^{\mathbf{q}}_{\mathrm{sp}}(, i\omega_0)$ (*SI Appendix*, Fig. S14).

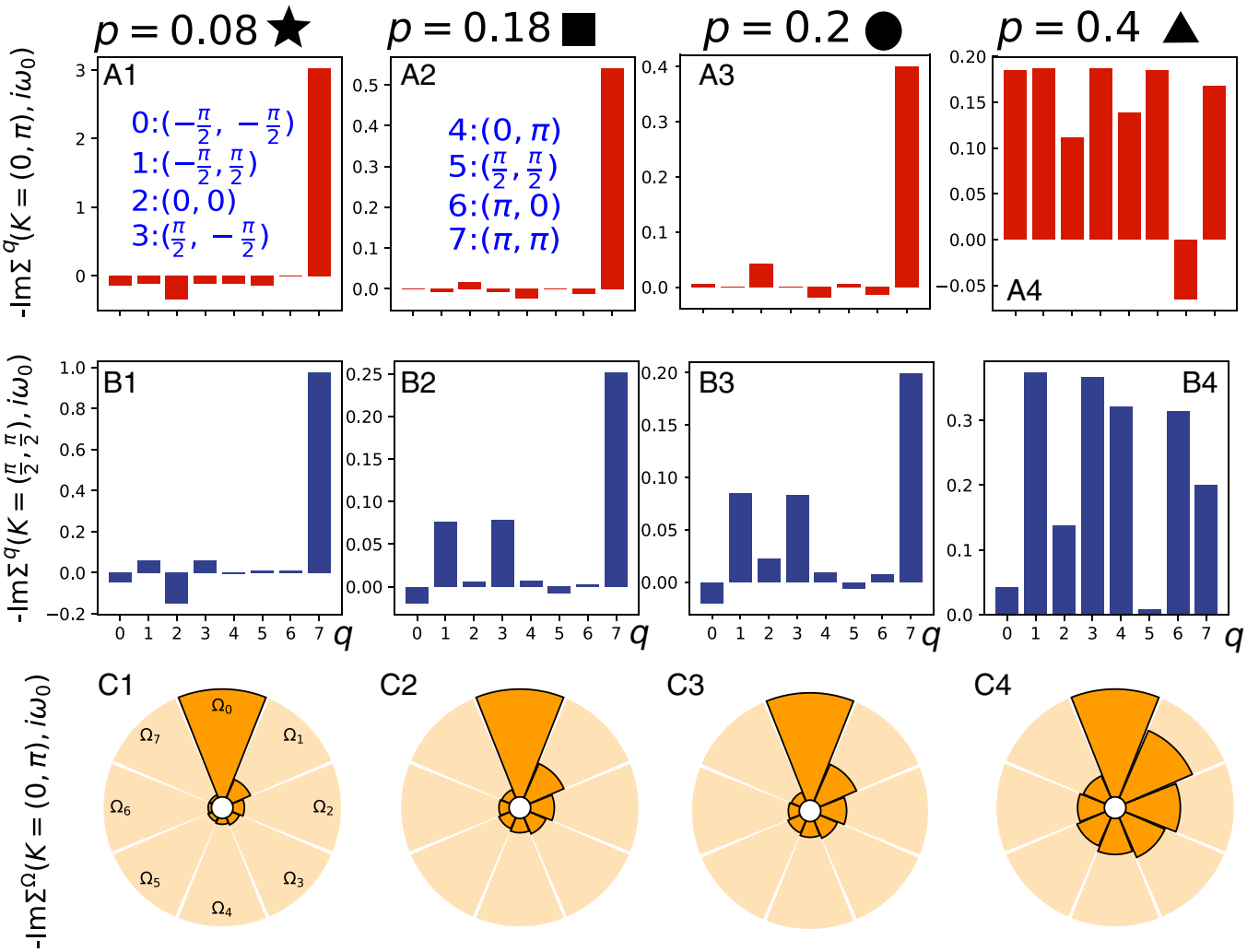

Fig. 4. The fluctuation diagnostic (Dyson–Schwinger equation of motion decomposition) of the self-energy in the spin channel, $\mathrm{Im}\Sigma_{sp}^{\mathbf{q}/\Omega_n}(\mathbf{k}, i\omega_0)$ at different dopings. (*A1–A4*) $\mathrm{Im}\Sigma_{sp}^{\mathbf{q}}(\mathbf{k}, i\omega_0)$ as a function of transfer momentum $\mathbf{q}$ for the antinode [$\mathbf{k} = (0, \pi)$]. (*B1–B4*) $\mathrm{Im}\Sigma_{sp}^{\mathbf{q}}(\mathbf{k}, i\omega_0)$ as a function of transfer momentum $\mathbf{q}$ for the node [$\mathbf{k} = (\pi/2, \pi/2)$]. (*C1–C4*) $\mathrm{Im}\Sigma_{sp}^{\Omega_n}(k, i\omega_0)$ as a function of transfer frequencies $\Omega_n = 2n\pi T$ for the antinode [$\mathbf{k} = (0, \pi)$] [values are renormalized by $\mathrm{Im}\Sigma_{sp}^{\Omega_0}(k, i\omega_0)$]. Values of indexes for transfer momenta $\mathbf{q}$ are labeled in *A1* and *A2*. $\mathrm{Im}\Sigma_{sp}^{\Omega_n}(k, i\omega_0)$ for the node, not shown here, is similar to that for the antinode (*C1–C4*).

emanating from a zero T QCP. This result differs essentially from ours since here we find a finite-doping range displaying T linearity as $T \to 0$.

Where does the linear T dependence come from? In the case of phonons, when temperature T is larger than about one-third of the Debye frequency (6), The scattering rate increases like T because the number of bosonic scatterers grows linearly with T (66). In the case of an antiferromagnetic QCP (16, 18–21), the characteristic spin fluctuation frequency plays the role of the Debye frequency in the phonon case and it indeed vanishes. However, it does not explain the T-linear scattering rate in the case of weak interactions, since the electrons–spin fluctuations scattering will be strong only at hot spots on the Fermi surface so that, barring disorder effects (67), the resulting resistivity will be short circuited by Fermi-liquid–like portions of the Fermi surface (68).

For the strong interaction, $U = 7t$ that we considered, it can be speculated that the lack of well-defined fermion quasiparticles leads to spin fluctuations with overall vanishing characteristic frequency. Then, the argument that the number of scatterers scales like T should hold. Since the magnetic correlation length is small in the overdoped regime (69), the electrons on remains of the Fermi surface can be all effectively scattered. Then the argument that the linear T dependence of the scattering rate is isotropic on the Fermi surface will also hold. In this case, dimensional analysis and Kanamori–Brückner screening (70, 71) suggest (*SI Appendix*, section L) that the coefficient of the linear T dependence of the scattering rate can be of order unity. But it does not need to be unity. In fact, we find a number about equal to 3 for the electron-scattering rate and about $(1 \sim 2)$ for the quasiparticle-scattering rate with the current parameters. So we call the strong-interaction case that we studied a "nearly Planckian liquid" and we argue that Planckian dissipation is likely not a fundamental limit to the inelastic electron-scattering rate (66, 72).

Conclusion

We investigated the two-dimensional Hubbard model in the intermediate to strong interaction limit where a non-Fermi liquid phase is found to exist in the overdoped regime. We found that the electronic scattering rate $\gamma_k(T)$ can have a perfectly linear T dependence when doping p is close to the pseudogap critical doping p^*. We also discovered that the antiferromagnetic fluctuations are responsible for the T-linear electron scattering at low temperatures.

Materials and Methods

Our results for the two-dimensional Hubbard model are obtained using the DCA (44), which is a cluster extension of the DMFT. (See *SI Appendix*, sections A–C for details) The DCA method captures short-ranged spatial correlations within the cluster exactly, while longer-range spatial correlations are taken into account by a dynamical mean field, which can be represented by a momentum- and frequency-dependent Weiss field $g_0(\mathbf{k}, i\omega_n)$. The effective cluster impurity problem starting from $g_0(\mathbf{k}, i\omega_n)$ is solved by the Hirsch–Fye quantum Monte Carlo method (73), which in general has a slightly better average sign compared to the continuous-time quantum Monte Carlo (CTQMC) method (74). Here we use a discrete imaginary-time step $\Delta\tau = 0.071$. We have carefully verified that this finite $\Delta\tau$ is small enough so that the Trotter errors do not affect our result and conclusion (*SI Appendix*, Fig. S2). Comparison with the CTQMC result also shows that our conclusion is not changed in the $\Delta\tau \to 0$ limit (*SI Appendix*, Fig. S3). In this work, we typically use 60 DCA self-consistency iterations to get a converged Weiss field $g_0(\mathbf{k}, i\omega_n)$ or equivalently a converged self-energy $\Sigma(\mathbf{k}, i\omega_n)$. In the 8-site DCA approximation, the lattice self-energy is approximated by a patchwise-constant self-energy $\Sigma(\mathbf{k}, i\omega_n)$ in the Brillouin zone with eight different patches as shown in *SI Appendix*, Fig. S1. Note that the antinodal and nodal regions are in distinct patches in this 8-site cluster scheme. We have verified that the *T*-linear scattering rate also appears in 4-site DCA and 4×4-site DCA calculations; namely, it can be checked explicitly for $T > 0.1$ that our results are insensitive to the cluster size (*SI Appendix*, Figs. S16 and S17).

Data Availability. Data have been deposited in the Open Science Framework repository, https://osf.io/zmnsd/.

ACKNOWLEDGMENTS. This work has been supported by the National Natural Science Foundation of China (Grant 41030053), by the Natural Science Foundation of Guangdong Province (Grant 42030030), by the Natural Sciences and Engineering Research Council of Canada under Grant RGPIN-2019-05312, and by the Canada First Research Excellence Fund. We acknowledge discussions with Andrey Chubukov, Nigel Hussey, Jake Ayres, Antoine Georges, Michel Ferrero, and Nils Wentzell. Part of the computational work was carried out at the National Supercomputer Center in Guangzhou (TianHe-2).

Author affiliations: [a]School of Physics, Sun Yat-sen University, Guangzhou, 510275, Guangdong, China; and [b]Département de Physique, Institut Quantique and Regroupement Québécois sur les Matériaux de Pointe, Université de Sherbrooke, Sherbrooke, QC J1K 2R1, Canada

1. G. R. Stewart, Non-fermi-liquid behavior in *d*- and *f*-electron metals. *Rev. Mod. Phys.* **73**, 797–855 (2001).
2. A. Legros *et al.*, Universal *T*-linear resistivity and Planckian dissipation in overdoped cuprates. *Nat. Phys.* **15**, 142–147 (2019).
3. J. Zaanen *et al.*, Planckian dissipation, minimal viscosity and the transport in cuprate strange metals. *SciPost Phys.* **6**, 61 (2019).
4. B. Shen *et al.*, Strange-metal behaviour in a pure ferromagnetic Kondo lattice. *Nature* **579**, 51–55 (2020).
5. C. M. Varma, Colloquium: Linear in temperature resistivity and associated mysteries including high temperature superconductivity. *Rev. Mod. Phys.* **92**, 031001 (2020).
6. S. A. Hartnoll, A. P. Mackenzie, Planckian dissipation in metals. arXiv [Preprint] (2021). https://arxiv.org/abs/2107.07802 (Accessed 18 March 2022).
7. J. Ayres *et al.*, Incoherent transport across the strange-metal regime of overdoped cuprates. *Nature* **595**, 661–666 (2021).
8. R. A. Cooper et al., Anomalous criticality in the electrical resistivity of $La_2 - xSr_xCuO_4$. *Science* **323**, 603–607 (2009).
9. R. Daou *et al.*, Linear temperature dependence of resistivity and change in the Fermi surface at the pseudogap critical point of a high-Tc superconductor. *Nat. Phys.* **5**, 31–34 (2009).
10. N. E. Hussey *et al.*, Dichotomy in the T-linear resistivity in hole-doped cuprates. *Philos. Trans. R. Soc. A* **369**, 1626–1639 (2011).
11. H. v. Löhneysen *et al.*, Non-Fermi-liquid behavior in a heavy-fermion alloy at a magnetic instability. *Phys. Rev. Lett.* **72**, 3262–3265 (1994).
12. S. A. Grigera *et al.*, Magnetic field-tuned quantum criticality in the metallic ruthenate Sr3Ru2O7. *Science* **294**, 329–332 (2001).
13. N. Doiron-Leyraud *et al.*, Correlation between linear resistivity and T_c in the bechgaard salts and the pnictide superconductor $Ba(Fe_{1-x}Co_x)_2As_2$. *Phys. Rev. B Condens. Matter Mater. Phys.* **80**, 214531 (2009).
14. C. M. Varma, P. B. Littlewood, S. Schmitt-Rink, E. Abrahams, A. E. Ruckenstein, Phenomenology of the normal state of Cu-O high-temperature superconductors. *Phys. Rev. Lett.* **63**, 1996–1999 (1989).
15. T. M. Rice, N. J. Robinson, A. M. Tsvelik, Umklapp scattering as the origin of *T*-linear resistivity in the normal state of high-T_c cuprate superconductors. *Phys. Rev. B* **96**, 220502 (2017).
16. A. J. Millis, Effect of a nonzero temperature on quantum critical points in itinerant fermion systems. *Phys. Rev. B Condens. Matter* **48**, 7183–7196 (1993).
17. A. Abanov, A. V. Chubukov, J. Schmalian, Quantum-critical theory of the spin-fermion model and its application to cuprates: Normal state analysis. *Adv. Phys.* **52**, 119–218 (2003).
18. P. Gegenwart, Q. Si, F. Steglich, Quantum criticality in heavy-fermion metals. *Nat. Phys.* **4**, 186–197 (2008).
19. H. v. Löhneysen, A. Rosch, M. Vojta, P. Wölfle, Fermi-liquid instabilities at magnetic quantum phase transitions. *Rev. Mod. Phys.* **79**, 1015–1075 (2007).
20. X. Y. Xu, A. Klein, K. Sun, A. V. Chubukov, Z. Y. Meng (2020) Identification of non-fermi liquid fermionic self-energy from quantum monte carlo data. *npj Quantum Mater.* **5**, 65.
21. P. T. Dumitrescu, N. Wentzell, A. Georges, O. Parcollet, Planckian metal at a doping-induced quantum critical point. arXiv [Preprint] (2021). https://arxiv.org/abs/2103.08607 (Accessed 18 March 2022).
22. P. Cha, N. Wentzell, O. Parcollet, A. Georges, E. A. Kim, Linear resistivity and Sachdev-Ye-Kitaev (SYK) spin liquid behavior in a quantum critical metal with spin-1/2 fermions. *Proc. Natl. Acad. Sci. U.S.A.* **117**, 18341–18346 (2020).
23. S. Sachdev, J. Ye, Gapless spin-fluid ground state in a random quantum Heisenberg magnet. *Phys. Rev. Lett.* **70**, 3339–3342 (1993).
24. A. A. Patel, S. Sachdev, Theory of a Planckian metal. *Phys. Rev. Lett.* **123**, 066601 (2019).
25. O. Parcollet, A. Georges, Non-fermi-liquid regime of a doped Mott insulator. *Phys. Rev. B* **59**, 5341 (1999).
26. D. J. Scalapino, "Numerical studies of the 2D Hubbard model" in *Handbook of High-Temperature Superconductivity: Theory and Experiment*, J. R. Schrieffer, J. S. Brooks, Eds. (Springer New York, 2007), pp. 495–526.
27. T. A. Maier, M. Jarrell, T. C. Schulthess, P. R. C. Kent, J. B. White, Systematic study of d-wave superconductivity in the 2D repulsive Hubbard model. *Phys. Rev. Lett.* **95**, 237001 (2005).
28. E. Gull, O. Parcollet, A. J. Millis, Superconductivity and the pseudogap in the two-dimensional Hubbard model. *Phys. Rev. Lett.* **110**, 216405 (2013).
29. L. Fratino, P. Sémon, G. Sordi, A. M. Tremblay, An organizing principle for two-dimensional strongly correlated superconductivity. *Sci. Rep.* **6**, 22715 (2016).
30. A. Macridin, M. Jarrell, T. Maier, P. R. C. Kent, E. D'Azevedo, Pseudogap and antiferromagnetic correlations in the Hubbard model. *Phys. Rev. Lett.* **97**, 036401 (2006).
31. D. Sénéchal, A. M. S. Tremblay, Hot spots and pseudogaps for hole- and electron-doped high-temperature superconductors. *Phys. Rev. Lett.* **92**, 126401 (2004).
32. G. Sordi, P. Sémon, K. Haule, A. M. S. Tremblay, Pseudogap temperature as a Widom line in doped Mott insulators. *Sci. Rep.* **2**, 1–5 (2012).
33. W. Wu *et al.*, Pseudogap and Fermi-surface topology in the two-dimensional Hubbard model. *Phys. Rev. X* **8**, 021048 (2018).
34. A. Reymbaut *et al.*, Pseudogap, Van Hove singularity, maximum in entropy, and specific heat for hole-doped Mott insulators. *Phys. Rev. Res.* **1**, 023015 (2019).
35. W. Wu, M. S. Scheurer, M. Ferrero, A. Georges, Effect of Van Hove singularities in the onset of pseudogap states in Mott insulators. *Phys. Rev. Res.* **2**, 033067 (2020).
36. B. X. Zheng *et al.*, Stripe order in the underdoped region of the two-dimensional Hubbard model. *Science* **358**, 1155–1160 (2017).
37. S. S. Dash, D. Sénéchal, Charge- and pair-density-wave orders in the one-band Hubbard model from dynamical mean field theory. *Phys. Rev. B* **103**, 045142 (2020).
38. E. Perepelitsky *et al.*, Transport and optical conductivity in the Hubbard model: A high-temperature expansion perspective. *Phys. Rev. B* **94**, 235115 (2016).
39. E. W. Huang, R. Sheppard, B. Moritz, T. P. Devereaux, Strange metallicity in the doped Hubbard model. *Science* **366**, 987–990 (2019).
40. P. Cha, A. A. Patel, E. Gull, E. A. Kim, Slope invariant *T*-linear resistivity from local self-energy. *Phys. Rev. Res.* **2**, 033434 (2020).
41. P. T. Brown *et al.*, Bad metallic transport in a cold atom Fermi-Hubbard system. *Science* **363**, 379–382 (2019).
42. O. Gunnarsson, M. Calandra, J. E. Han, Colloquium: Saturation of electrical resistivity. *Rev. Mod. Phys.* **75**, 1085–1099 (2003).
43. G. Grissonnanche *et al.*, Linear-in temperature resistivity from an isotropic Planckian scattering rate. *Nature* **595**, 667–672 (2021).
44. T. Maier, M. Jarrell, T. Pruschke, M. H. Hettler, Quantum cluster theories. *Rev. Mod. Phys.* **77**, 1027–1080 (2005).
45. S. D. Chen *et al.*, Incoherent strange metal sharply bounded by a critical doping in Bi2212. *Science* **366**, 1099–1102 (2019).
46. E. Pavarini, I. Dasgupta, T. Saha-Dasgupta, O. Jepsen, O. K. Andersen, Band-structure trend in hole-doped cuprates and correlation with T(c max). *Phys. Rev. Lett.* **87**, 047003 (2001).
47. A. Georges, G. Kotliar, W. Krauth, M. J. Rozenberg, Dynamical mean-field theory of strongly correlated fermion systems and the limit of infinite dimensions. *Rev. Mod. Phys.* **68**, 13–125 (1996).
48. N. Barišić *et al.*, Universal sheet resistance and revised phase diagram of the cuprate high-temperature superconductors. *Proc. Natl. Acad. Sci. U.S.A.* **110**, 12235–12240 (2013).
49. A. Schröder *et al.*, Onset of antiferromagnetism in heavy-fermion metals. *Nature* **407**, 351–355 (2000).
50. T. Schäfer *et al.*, Tracking the footprints of spin fluctuations: A multimethod, multimessenger study of the two-dimensional Hubbard model. *Phys. Rev. X* **11**, 011058 (2021).
51. S. Sachdev, *Quantum Phase Transitions* (Cambridge University Press, ed. 2, 2011).
52. O. Cyr-Choinière *et al.*, Pseudogap temperature T^* of cuprate superconductors from the Nernst effect. *Phys. Rev. B* **97**, 064502 (2018).
53. E. Gull, M. Ferrero, O. Parcollet, A. Georges, A. J. Millis, Momentum-space anisotropy and pseudogaps: A comparative cluster dynamical mean-field analysis of the doping-driven metal-insulator transition in the two-dimensional Hubbard model. *Phys. Rev. B Condens. Matter Mater. Phys.* **82**, 155101 (2010).
54. G. Sordi, P. Sémon, K. Haule, A. M. S. Tremblay, *c*-axis resistivity, pseudogap, superconductivity, and Widom line in doped Mott insulators. *Phys. Rev. B Condens. Matter Mater. Phys.* **87**, 041101 (2013).
55. W. Xu, K. Haule, G. Kotliar, Hidden Fermi liquid, scattering rate saturation, and Nernst effect: A dynamical mean-field theory perspective. *Phys. Rev. Lett.* **111**, 036401 (2013).
56. O. Gunnarsson *et al.*, Fluctuation diagnostics of the electron self-energy: Origin of the pseudogap physics. *Phys. Rev. Lett.* **114**, 236402 (2015).
57. W. Wu, M. Ferrero, A. Georges, E. Kozik, Controlling Feynman diagrammatic expansions: Physical nature of the pseudogap in the two-dimensional Hubbard model. *Phys. Rev. B* **96**, 041105(R) (2017).

58. X. Dong, X. Chen, E. Gull, Dynamical charge susceptibility in the Hubbard model. *Phys. Rev. B* **100**, 235107 (2019).
59. T. Schäfer, A. Toschi, How to read between the lines of electronic spectra: The diagnostics of fluctuations in strongly correlated electron systems. *J. Phys. Condens. Matter* **33**, 214001 (2021).
60. S. Wakimoto *et al.*, Disappearance of antiferromagnetic spin excitations in overdoped $la_{2-x}sr_xcuo_4$. *Phys. Rev. Lett.* **98**, 247003 (2007).
61. M. Le Tacon *et al.*, Dispersive spin excitations in highly overdoped cuprates revealed by resonant inelastic x-ray scattering. *Phys. Rev. B* **88**, 020501 (2013).
62. A. Kaminski *et al.*, Momentum anisotropy of the scattering rate in cuprate superconductors. *Phys. Rev. B* **71**, 014517 (2005).
63. X. Deng *et al.*, How bad metals turn good: Spectroscopic signatures of resilient quasiparticles. *Phys. Rev. Lett.* **110**, 086401 (2013).
64. D. Chowdhury, A. Georges, O. Parcollet, S. Sachdev, Sachdev-Ye-Kitaev models and beyond: A window into non-Fermi liquids. arXiv [Preprint] (2021). https://arxiv.org/abs/2109.05037 (Accessed 18 March 2022).
65. N. S. Vidhyadhiraja, A. Macridin, C. Şen, M. Jarrell, M. Ma, Quantum critical point at finite doping in the 2D Hubbard model: A dynamical cluster quantum Monte Carlo study. *Phys. Rev. Lett.* **102**, 206407 (2009).
66. M. V. Sadovskii, Planckian relaxation delusion in metals. *Phys. Uspekhi* **64**, 175–190 (2021).
67. A. Rosch, Interplay of disorder and spin fluctuations in the resistivity near a quantum critical point. *Phys. Rev. Lett.* **82**, 4280–4283 (1999).
68. R. Hlubina, T. M. Rice, Resistivity as a function of temperature for models with hot spots on the Fermi surface. *Phys. Rev. B Condens. Matter* **51**, 9253–9260 (1995).
69. M. A. Kastner, R. J. Birgeneau, G. Shirane, Y. Endoh, Magnetic, transport, and optical properties of monolayer copper oxides. *Rev. Mod. Phys.* **70**, 897–928 (1998).
70. J. Kanamori, Electron correlation and ferromagnetism of transition metals. *Prog. Theor. Phys.* **30**, 275–289 (1963).
71. K. A. Brueckner, T. Soda, P. W. Anderson, P. Morel, Level structure of nuclear matter and liquid he^3. *Phys. Rev.* **118**, 1442–1446 (1960).
72. J. Yuan *et al.*, Scaling of the strange-metal scattering in unconventional superconductors. *Nature* **602**, 431–436 (2022).
73. J. E. Hirsch, R. M. Fye, Monte Carlo method for magnetic impurities in metals. *Phys. Rev. Lett.* **56**, 2521–2524 (1986).
74. E. Gull *et al.*, Continuous-time Monte Carlo methods for quantum impurity models. *Rev. Mod. Phys.* **83**, 349–404 (2011).